Compact high-aperture interferometer with a diffractive reference wave for high-precision referenceless aberration measurements of optical elements and systems

A.A. Akhsakhalyan [a], N.I. Chkhalo [a,*], N. Kumar [a], I.V. Malyshev [a], A.E. Pestov [a], N. N. Salashchenko [a], M.N. Toropov [a], B.A. Ulasevich [a], S.V. Kuzin [b]

[a] *Institute for Physics of Microstructures RAS, 603950, GSP-105, Nizhny Novgorod, Russia*
[b] *P.N. Lebedev Physical Institute of RAS, 119991, GSP-1 Moscow, Leninsky prospect, 53, Russia*

ARTICLE INFO

ABSTRACT

We present the optical layout and actual design of a compact high-aperture referenceless point diffraction interferometer with a diffraction reference wave. The basic concept of this interferometer is based on a single-mode optical fibre with a subwave output aperture, which is used as a source of spherical reference waves. The interferometer is designed for high-precision measurements of the surface shape and aberrations of optical elements. It makes use of a diffraction reference wave and is developed for mass industrial applications. The proposed design does not require the involvement of special external conditions, and reduces the need for calibrated reference surfaces. We evaluate the performance of our interferometer for highprecision measurements and demonstrate its use by presenting results obtained from measuring the shapes of spherical references from various manufacturers and the aberration of a five lens objective.

1. Introduction

Interferometry is the main tool used for optical elements and systems, both at the manufacturing stage and at the final stage of certification. It can provide precision measurements of the shapes of optical surfaces and the aberrations in optical systems. The most common types are Michelson, Fizeau and Twyman-Green interferometers [1]. However, the main drawback of these interferometers is their reliance on reference surfaces to create a reference wave, which interferes with the working front that is reflected or passed through the workpiece under study and which carries information about all its defects. Reference surfaces, as a rule, introduce basic uncertainties into the measurements of the absolute values of aberrations, and manufacturers of advanced interferometric equipment report the high reproducibility of measurements of up to $\lambda/10000$, with rather moderate absolute values of $\lambda/20 - \lambda/100$ [2]. At a nanometre level of accuracy, the error when measuring the absolute values of aberrations includes not only the errors in the manufacture of the reference shape, but also the method of its installation in the interferometer and the possible aging of the metal rims. Hence, when the development of EUV lithography began to require

optics with an accuracy better than 1 nm [3], the developers of optics equipment turned to referenceless interferometry.

The use of light diffraction with an aperture of small size (comparable to the wavelength) to generate a diverging spherical wave that can be used in interferometric measurements as a reference wave was first proposed in Ref. [4]. Since the diffraction of light at a small aperture falls into the class of electrodynamic problems that can be solved with predetermined accuracy, including the optical constants of the screen material and the irregularities of the aperture, this method of generating a reference spherical wave can be referred to as *ab initio*.

A few interferometers based on this principle, later called point diffraction interferometers (PDIs), were manufactured in laboratories for various applications. Sub-nanometre measurement accuracy was demonstrated for the first time in Ref. [5]. This interferometer used a single-mode optical fibre core as a reference spherical wave source (RSWS). The disadvantage of this interferometer was its low numerical aperture (NA≈0.1), since the core had a diameter of d ≈ 4 μm and the angular width of the diffraction peak is $\pm\lambda/d$.

Large angular apertures have an RSWS that is based on the diffraction of light from a small aperture in an opaque screen [6–10]. A

---

* Corresponding author.
  E-mail address: chkhalo@ipmras.ru (N.I. Chkhalo).
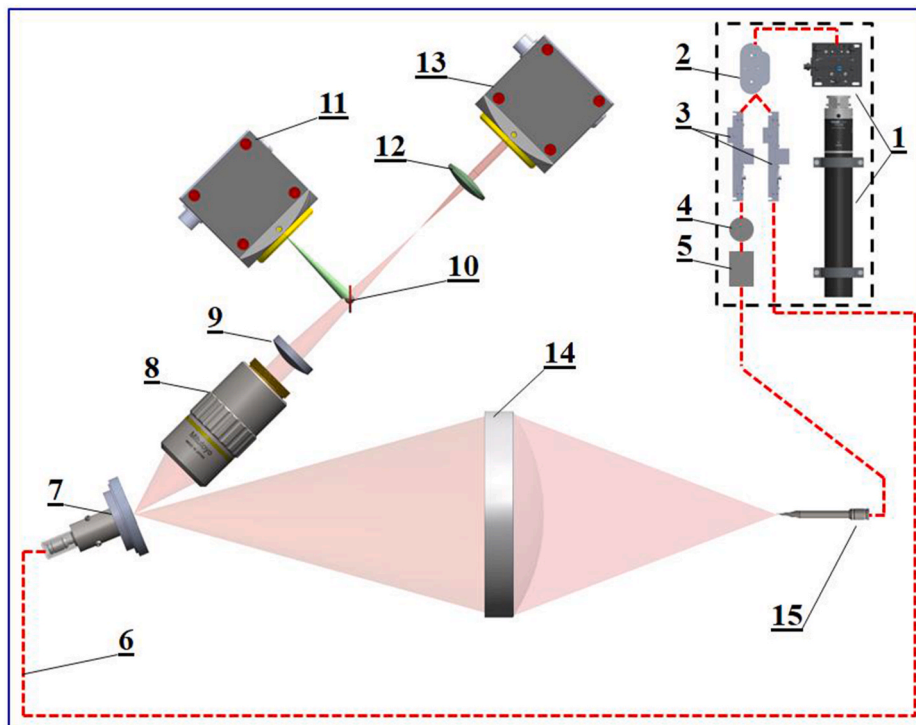
Fig. 1. Optical layout of the interferometer: (1) laser with a magneto-optical isolator and an optical system for focusing the laser radiation into the beam splitter; (2) fibre-optic beam splitter; (3) polarisation controllers; (4) phase-shifting element; (5) light intensity attenuator; (6) single-mode optical fibre connected to TSMOF #1; (7) TSMOF and flat mirror module inserted into a piezoelectric phase-shifting element; (8) lens; (9) and (12) plano-convex lenses; (10) movable flat mirror; (11) CCD camera #1; (13) CCD camera #2; (14) investigated detail; (15) TSMOF #2.
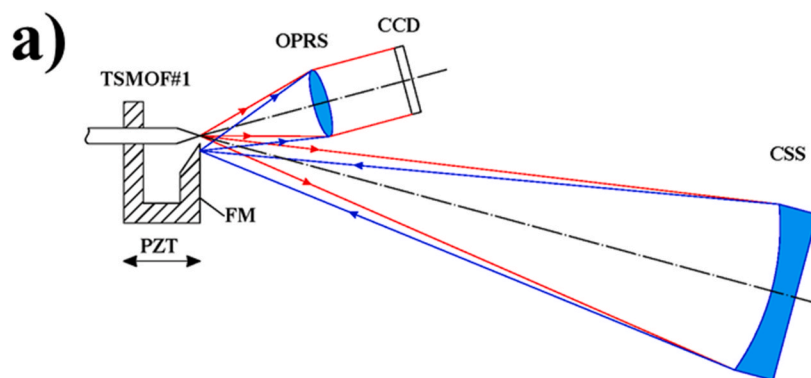
Fig. 2. (a) Diagram and (b) photograph of the interferometer in the process of measuring a spherical concave part.

compromise between a sufficiently large working numerical aperture and the intensity of the spherical wave can be achieved with a pinhole of size 0.5 μm ($\lambda/d > 1$), except an interferometer at ALS synchrotron with an operating wavelength of 13.5 nm [7]. However, these interferometers also have a number of drawbacks that limit their working aperture and the quality of the diffraction reference wave. In Ref. [8], it was noted that the aberrations of a spherical wave generated by the diffraction of light by a pinhole are affected by the aberrations of the primary optics that focus the light at the hole. They are also affected by a slight shift in the axes of the laser beam and the pinhole relative to each other. The effect of these errors is reduced with a decrease in the diameter of the pinhole, but the quadratic reduction in the intensity of the wave does not allow this to happen. Another problem is related to the angular nonuniformity of the intensity of the diffraction wave, which leads to a shift in the coordinates towards the extremes of the interference pattern.

The working aperture and the intensity of the spherical wave were noticeably increased by the use of a single-mode optical fibre with a sub-wave output aperture (TSMOF - tipped single mode optical fibre) as a reference spherical wave source [11]. In this case, the laser radiation was fed into an optical fibre with a core diameter of about 4 μm, which improved the efficiency of the laser radiation power by up to 50% [12]. An eigenmode was formed in the waveguide that prevented the influence of the primary optics from affecting the quality of the diffracted wave. The interferometric and recording parts consisted of a TSMOF, a CCD matrix, and a lens that collected the reference and working fronts. This made it possible to carry out measurements in a vacuum environment or atmosphere-controlled chamber into which light was introduced through a fibre-optic cable [13]. The use of TSMOF also allows several coherent waves to be produced.

Several laboratory interferometers have been developed recently based on this type of light source, with the aim of resolving numerous problems such as measurements of the surface shape and the aberrations of optical systems, reference-free measurements of roughness in the mid-frequency range [14], and linear displacements [12,15]. A number of theoretical and experimental analyses [12,16] have also been carried out for wavefronts generated using a TSMOF.

However, an interferometer based on a high-aperture TSMOF for industrial applications has not yet been developed, perhaps due to the lack of a reference spherical wave source on the market with the required wavefront characteristics. In this work, a device is developed in which almost all the major problems with PDIs are resolved. This was achieved after several years of collective effort by our research group on the development and scientific application of PDIs. Our instrument, which can provide sub-nanometre measurement accuracy, is ready for commercial production.

2. Design principles and fabrication of the interferometer

The design concept is based on widely used fibre-optic components. As a source of the spherical reference wave, we use TSMOFs, whose tips are made by chemical etching [11]. This method provides a smaller aperture diameter (tens of nanometres [17]) compared with thermoplastic stretching. According to rigorous electromagnetic calculations [12], a smaller aperture leads to an increase in the working aperture and a decrease in the aberration of the spherical wave. The interaction of light with the metal film at the edge of the aperture is considered to be one of the leading factors affecting the aberration of the diffracted wave [18]. The convex shape of the tip increases the viewing angle at which the light rays start to pass through the film.

The basic optical layout of the interferometer is shown in Fig. 1. An He:Ne laser with stable optical power and wavelength is used for the radiation source (1). A magneto-optical isolator is installed at the laser output, which basically protects the laser cavity from light reflected from the other optical elements, which can lead to instability in the radiation characteristics. After the optical isolator, the light enters an aspherical lens which is mounted on a five-axis table. By adjusting the

table, the focus of the lens and the input end of the single-mode optical fibre can be aligned. Light is wound into the fibre with an efficiency of about 75%. The light then enters the fibre-optic beam splitter (2), where it is split into two coherent channels, each with an intensity of 1:1. The light in each channel hits the fibre-optic polarisation controllers (3), which set the desired polarisation of the light at the channel output. Using a single-mode optical fibre (6), the light from the first channel enters TSMOF #1. TSMOF #1 and a flat mirror (FM) (see Fig. 2) are integrated into a single module that is installed in the phase-shifting element (7). The entire device (7) is installed on a five-coordinate table that allows for position adjustment of the interferometer.

The fibre section of the second channel is coiled onto a piezoceramic cylinder, and voltage is applied to the outer and inner surfaces of this cylinder (4), which then expands and stretches the fibre. This element therefore causes a phase shift between the spherical waves in the two channels. The second channel ends with an FC/PC optical connector, to allow the TSMOF #2 source (15), which is coherent with the first one, to be connected to it. The phase-shifting elements are controlled using a two-channel controller. Item 14 shows the sample under study.

The recording system consists of an input lens (8), two plano-convex lenses (9) and (12), a movable flat mirror (10), and two video cameras (11) and (13). Lens (8) is from the Mitutoyo Plano series, and provides an image of a point source at infinity. Lenses (9) and (12) create an image of the investigated object at a CCD video camera (13). This arrangement makes it possible to install a lens from the Mitutoyo series with a different working aperture, without changing the relative positions of the other optical elements.

A movable flat mirror (10) and a video camera (11) are used to adjust the investigated object. After adjusting the object, the mirror (10) is automatically removed and interferograms are recorded using the CCD camera (13). This greatly simplifies and speeds up the coarse settings for the sample under study. Further fine-tuning of the number of interferogram fringes and focusing can be carried out based on the measured interferograms.

Two main aspects were considered in the design of lenses (9) and (12) for the recording system. Firstly, they needed to minimise the aberrations of the wavefronts passing through them. This condition arises from the wedge between the interfering fronts that propagate through the lenses with a small spatial displacement. This displacement should not lead to additional phase incursions. Secondly, the lens system needed to compensate for coma aberration, since the sources of the reference and working fronts are displaced relative to the optical axis, and the resulting coma can negatively affect the accuracy of measurement for the investigated object. This problem can be bypassed by calibrating the coma of the recording system as described below; however, it is then necessary to strictly control the position of the fronts relative to each other, which in some critical cases is impossible due to the individual characteristics of the aberrations of the investigated object. For instance, the focusing spot of the working front increases if an object under study has a strong spherical aberration or astigmatism. In this case, it is necessary to move it away from the edge of the FM, Fig. 2 a), to carry out precise measurements, and this automatically leads to a change in the distance between the sources.

We now consider the three main modes of operation of the interferometer in detail. The first mode is the attestation of single elements with concave spherical or weakly aspherical surfaces. As a rule, when the shape of the surface deviates from the nearest sphere by less than 1.5–2 μm, the interferogram can be reliably deciphered. In this case, the second channel and TSMOF #2 (position 15 in Fig. 1) are not used. Fig. 2 illustrates the method of operation of the interferometer, and shows the principle of measurement and a photograph of the interferometer in the first mode (a concave spherical surface measurement).

The TSMOF#1 portion of the spherical wavefront illuminates the workpiece (CSS), while the other part of the wavefront is directed to the recording system, consisting of an optical part (OPRS) and video camera (CCD). The wavefront reflected from the workpiece is focused on an FM
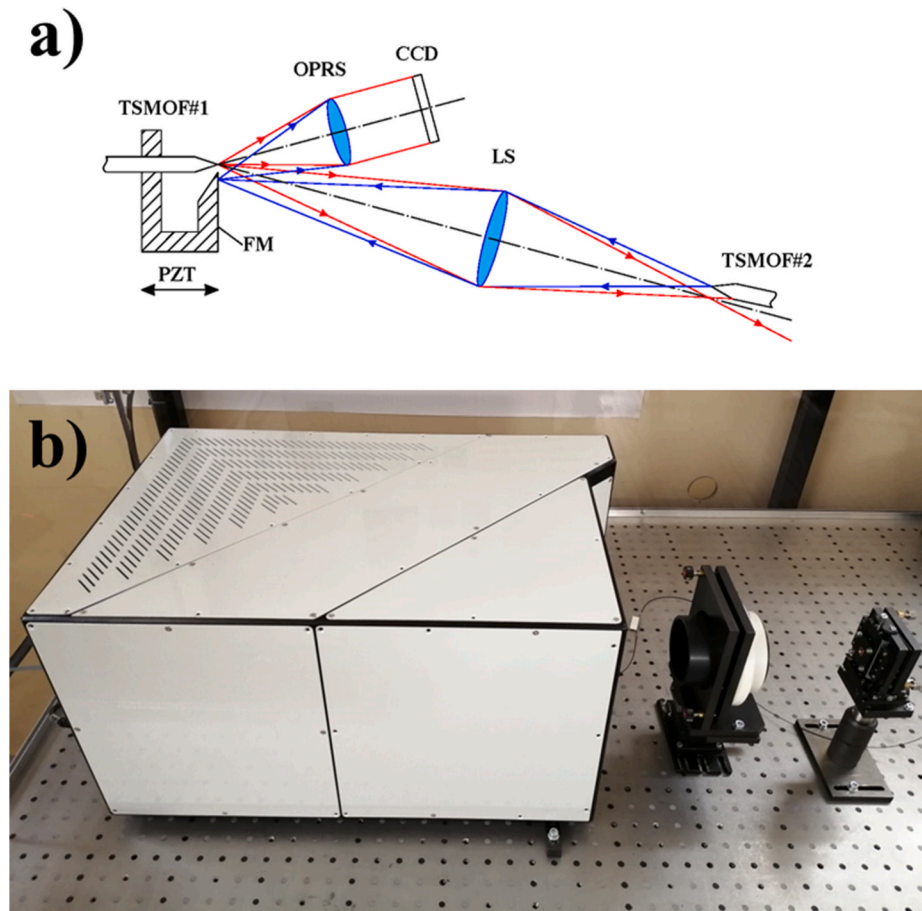
Fig. 3. (a) Diagram and (b) photograph of the interferometer in the process of measuring a five lens objective.

with a sharp edge in the immediate vicinity of the edge, and is also redirected to the recording system. Both fronts (reference and working) carry information about the errors of the investigated workpiece surface, and interfere in the plane of the CCD camera. TSMOF#1 and FM are integrated into a single module and mounted on a piezoelectric shifter (PZT) that creates a phase shift between the reference and working fronts.

The second basic mode involves the measurement of lenses and projection objectives. In this case, the investigated workpiece and the source of the spherical wave TSMOF#2 are set in relation to TSMOF#1 in such a way that both sources are located on the optical axis of the objective (lens) in the object and imaging planes, respectively. TSMOF#1 generates a reference wave, part of which is directed to the recording system, and the other part, which passes through the objective lens (LS), does not participate in interference. The reference spherical wave TSMOF#2 illuminates the LS, is deformed in accordance with the errors of the sample under study, and then interferes with the reference front of TSMOF#1, by analogy with reflective optics.

A similar measurement scheme is used to study ellipsoids, toroids, Schwarzschild and Kirkpatrick-Baez objectives, and other imaging systems. In this case, TSMOF#1 and TSMOF#2 are set at the foci (conjugate points) of the ellipsoid (toroid and other imaging systems).

To allow convex spherical surfaces to be measured as well as flat and strongly aspherical ones, a corresponding wavefront corrector is installed at the interferometer output. The corrector converts a diverging spherical front into a converging front (when studying a convex object), a flat front (when studying a flat object), or a diverging aspherical front in a shape that coincides with that of the investigated object. A diagram and photograph of the interferometer in the process of measuring a flat sample are shown in Fig. 4.

The overall dimensions of the interferometer are $300 \times 400 \times 600$ mm. The device can be operated with either a horizontal and vertical orientation of the optical axis. All of the movable elements of the interferometer are rigidly fixed in position along each of the axes.

3. Description and calibration of the main elements of the interferometer

3.1. Spherical reference wave source based on TSMOF

One key element that largely determines the unique capabilities of the interferometer is the spherical reference wave source based on a TSMOF with a sub-wavelength output aperture. Electron microscopic images of the TSMOF are shown in Fig. 5. The tipped end was created using a chemical etching method, and the metallisation of the sidewall surfaces was carried out by vacuum deposition. The optimal size of the output aperture to ensure a high intensity with a uniform distribution over the angle of the spherical wavefront is between 0.22 and 0.32 μm. The increase in the intensity of the laser at the fibre input is limited by thermal deformation of the TSMOF tip.

The final sampling sources for the interferometer was carried out in accordance with aberrations in Young's experiment. In this case, the interference pattern was recorded directly by the CCD camera without optical involvement (Fig. 6). The procedure used for source selection was as follows. One source was taken as a reference, and the aberrations of this source were measured together with others. The source for which the measured aberrations were the lowest was taken as the new standard, and the aberrations were then measured together with it. Sources for which the total aberration at numerical aperture of NA = 0.28 was less than 0.6 nm were considered suitable. The aberrations of individual
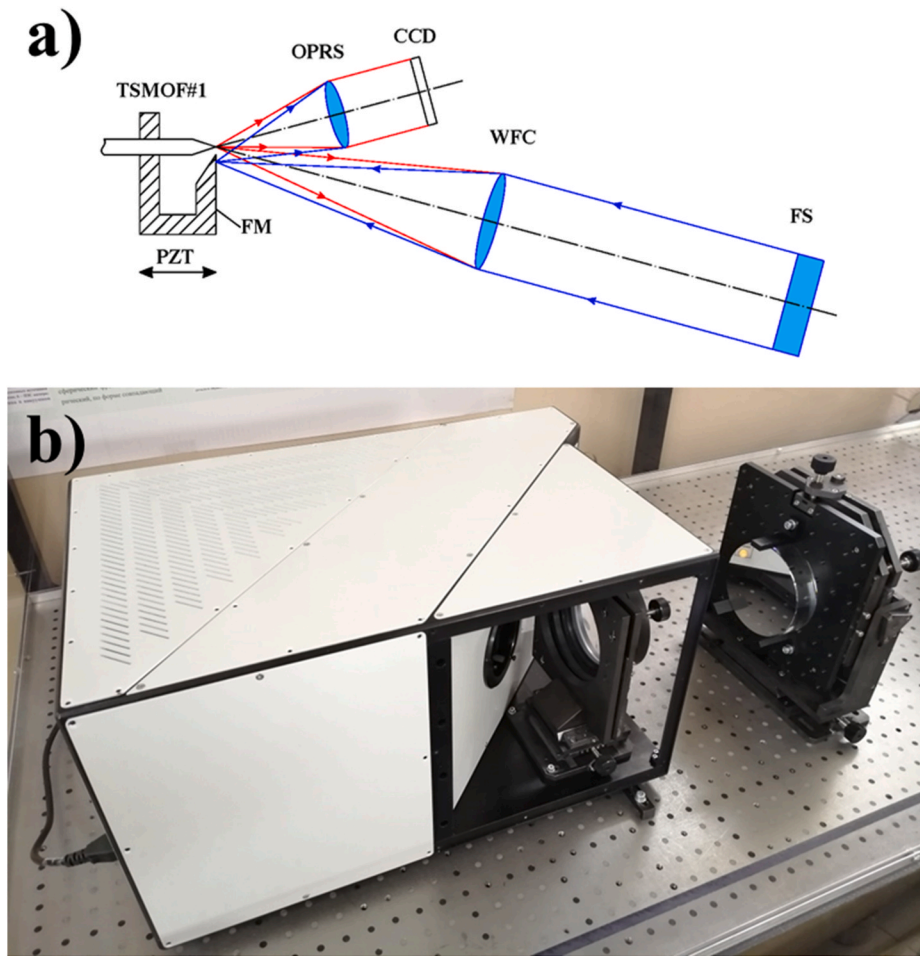
Fig. 4. (a) Diagram and (b) photograph of the interferometer in the process of measuring a. flat surface with using wave-front corrector.
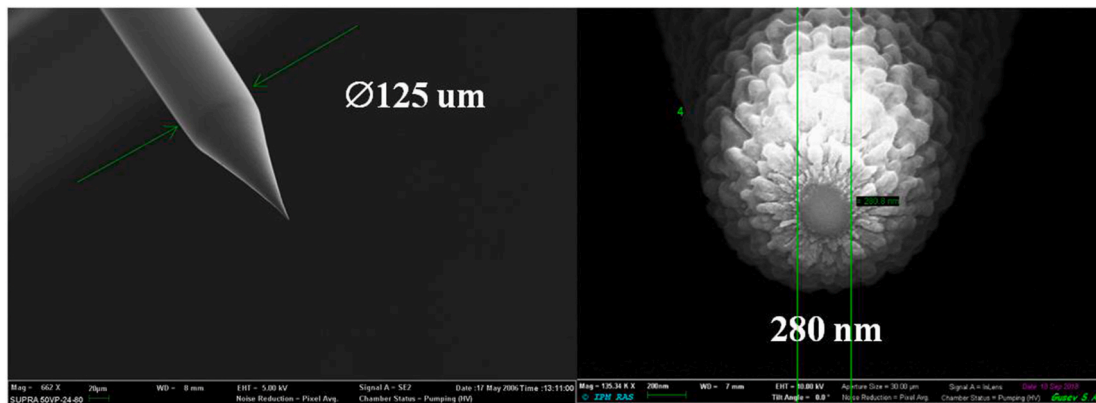
Fig. 5. Electron microscopic images of TSMOF based on single-mode optical fibre with sub-wavelength output aperture.

sources were not explored, although this could be done using the rotation technique discussed below.

In Fig. 7, the black square data points show the measured results for three positions of the CCD camera, corresponding to numerical apertures NA = 0.055, 0.14, and 0.28. It should be noted that due to the angle of 22° between the sources, in the experiment interfere the fronts generated in the angular aperture relative to TSMOF's axes up to NA = 0.46. The total aberration measured for two wavefronts with the maximum numerical aperture was around 0.5 nm.

It should be noted that at a sub-nanometre level of accuracy, aberrations will arise from an incorrectly aligned video camera, an incorrectly selected contour for the processing of interferograms, or the longitudinal displacement of one source relative to another. To eliminate these errors, the surface of the CCD video camera must be set strictly perpendicular to the axis passing through the centres of the interferogram and the line between the sources. This can be achieved using laser alignment: the laser beam is directed at the centre of the CCD, and the beam reflected in zero order (the brightest beam against which the two-dimensional diffraction pattern is visible) returns exactly to the laser. The weighted average coordinate of the laser beam will then
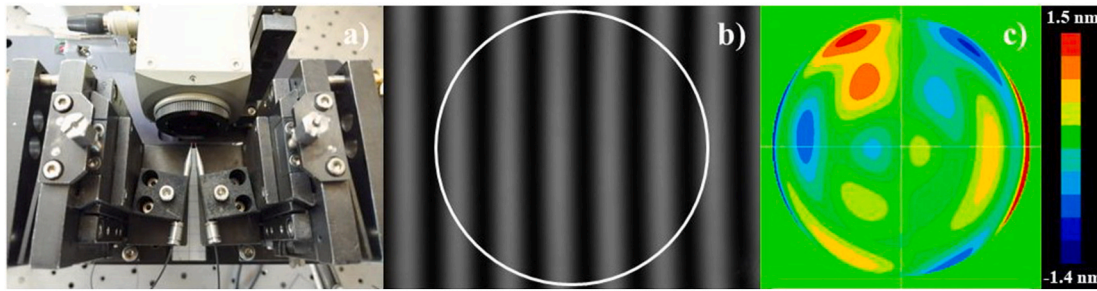
Fig. 6. (a) Photograph of Young's experiment, (b) the recorded interferogram and (c) the aberration map after subtracting the aberration of the coma associated with the shift in the sources relative to the optical axis of the system, calculated based on the known distance between the spherical wave sources and the detector and the number of interference fringes recorded.
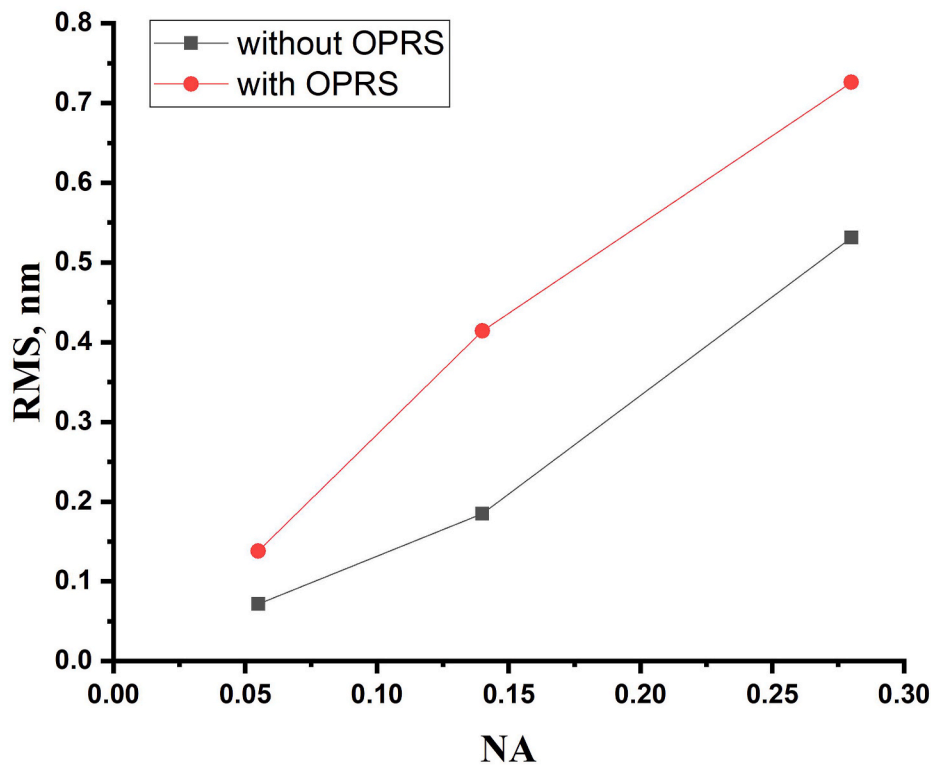
Fig. 7. Dependence of the total aberration of wavefronts of two TSMOFs on the numerical aperture: the upper curve shows the results in the presence of the optical part of the recording system (OPRS), and the lower curve shows the results without OPRS.

coincide with the centre of the interferogram. The sources are therefore set precisely at the centre of the laser beam. Control is applied based on the image of the shadow from one source and the number and orientation of interference fringes when the second TSMOF is set. As a rule, this alignment is sufficient to ensure that the aberrations caused by alignment errors are about 1 nm. Further fine adjustment of the position of the sources and the contour is carried out with interferometric controls: the defocusing aberration is minimised by moving one source relative to the other along the optical axis, and the astigmatism aberration is minimised by correcting the position of the centre of the contour.

The selected TSMOFs were integrated into a single module with a flat, sharp-edged mirror (see Figs. 2–4). A silicon wafer for the microelectronics was used as a substrate for the FM, which was coated on both sides with Si_3N_4 layers. When the required pattern had been created on the reverse of the silicon wafer via the lithography method and the removal of Si_3N_4, a sharp edge with an inclination angle of 54.7° was formed by anisotropic chemical etching. An aluminium reflective film was deposited onto the front surface of the substrate by magnetron sputtering. To reduce the roughness of the film, deposition was carried

out simultaneously from both Al and Si sources, where the fraction of Si was around 10%.

3.2. Recording system of the interferometer

The recording system is an important factor that can affect the measurement accuracy of the interferometer. As discussed above, the optical part of the recording system consists of a Mitutoyo lens and two plano-convex lenses, with dimensions matching those of the lens output diaphragm and the CCD matrix (Fig. 1).

In order to ensure sub-nanometre accuracy for the measurements, a numerical analysis carried out using Zemax software was used to confirm the mutual alignment of the optical elements of the interferometer with micrometre accuracy. To achieve this, all of the optical elements were installed on specially designed five-axis tables. Each degree of freedom of the stage was connected to the rigid fixture to ensure the long-term spatial stability of the optical elements. The positions of the optical elements were adjusted using interferometric measurements in the following way. In place of the TSMOF module (item 7 in Fig. 1),
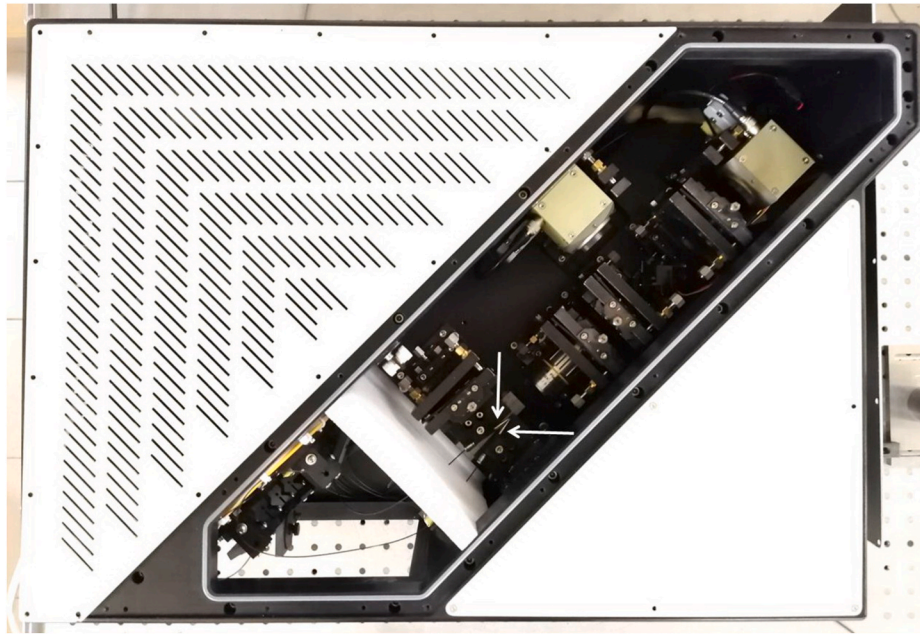
Fig. 8. Top photographic view of the interferometer. The two sources of the reference spherical wave are marked with white arrows.

two five-coordinate tables with two RSWSs were installed as shown in the photograph in Fig. 8. The top and side covers were removed to allow for approximate alignment using a laser, and precise alignment of all of the elements was then carried out via interferometric control.

For the ease of tuning, the wavefront aberrations $W(\overrightarrow{r})$ were represented in the form of a Zernike polynomial expansion [19]:

$$Z_n^m(r,\theta) = \sqrt{\frac{2(n+1)}{\pi(1+\delta_m^0)}} R_n^m(r) \Theta^m(\theta) \quad \text{circular Zernike polynomials} \tag{1}$$

where δ_m^0 is the Kronecker delta and

$$\Theta^m(\theta) = \begin{cases} \cos|m|\theta & (m > 0) \\ 1 & (m = 0) \\ \sin|m|\theta & (m < 0) \end{cases} \tag{2}$$

are angular functions.

$$R_n^m(r) = \sum_{s=0}^{(n-|m|)/2} \frac{(-1)^s (n-s)!}{s!\left(\frac{n+m}{2}-s\right)!\left(\frac{n-m}{2}-s\right)!} r^{n-2s} \tag{3}$$

are radial polynomials,

$$W(\overrightarrow{r}) = \sum_{n=0}^{\infty} \sum_{\substack{m=-n \\ m+=2}}^{n} c_{nm} Z_n^m(r,\theta) \tag{4}$$

is the expansion of function $W(\overrightarrow{r})$, and

$$c_{nm} = \iint_{r \leq 1} W(\overrightarrow{r}) Z_n^m(r,\theta) d^2\overrightarrow{r} \tag{5}$$

are the expansion coefficients of $W(\overrightarrow{r})$.

The use of this formalism can help us to analyse the contributions to the total wavefront of the various sources deforming the wavefront, since in the total expansion, the coefficients of the corresponding polynomials are simply summed as follows:

$$W(\overrightarrow{r}) = \sum_i W_i(r) \tag{6}$$
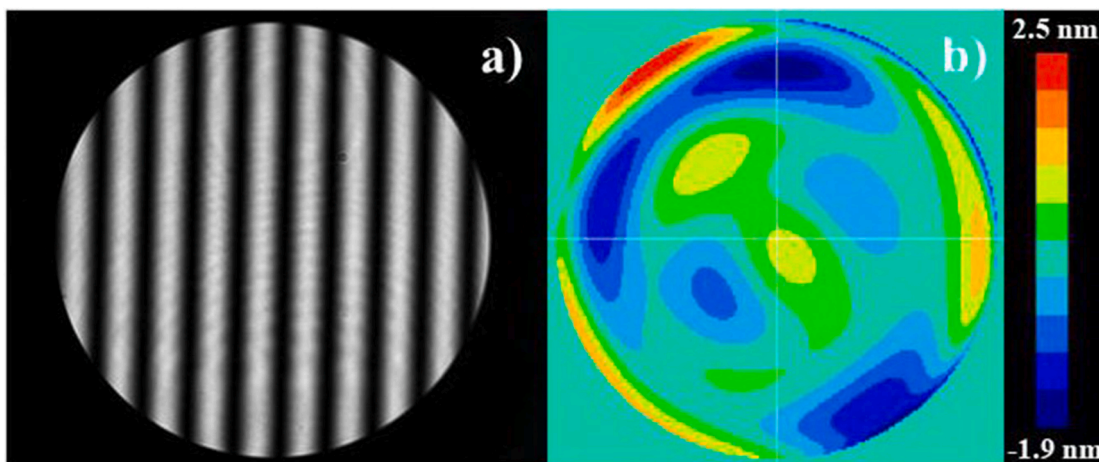
Fig. 9. (a) Measured interferogram and (b) aberration map with RMS = 0.7 nm and PV = 4.4 nm.
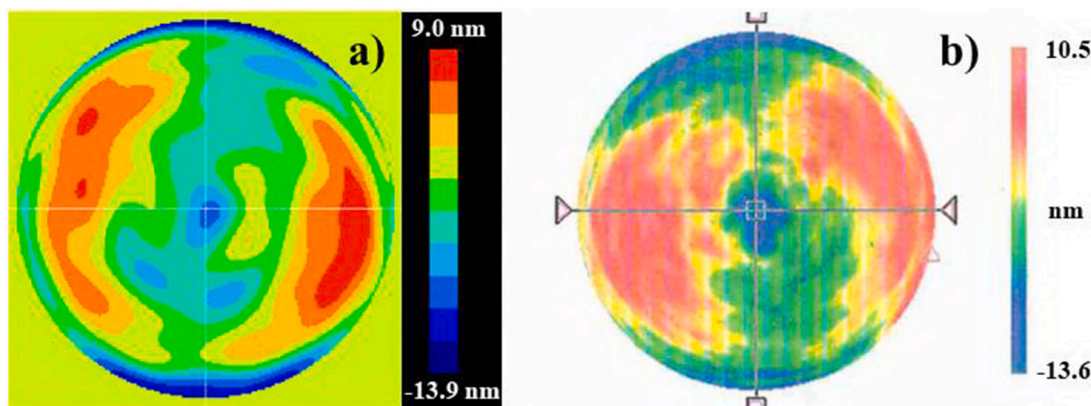
Fig. 10. Error map of the surface shape of the concave sphere of reference #1: (a) as measured by our interferometer, and (b) based on data provided by the manufacturer.
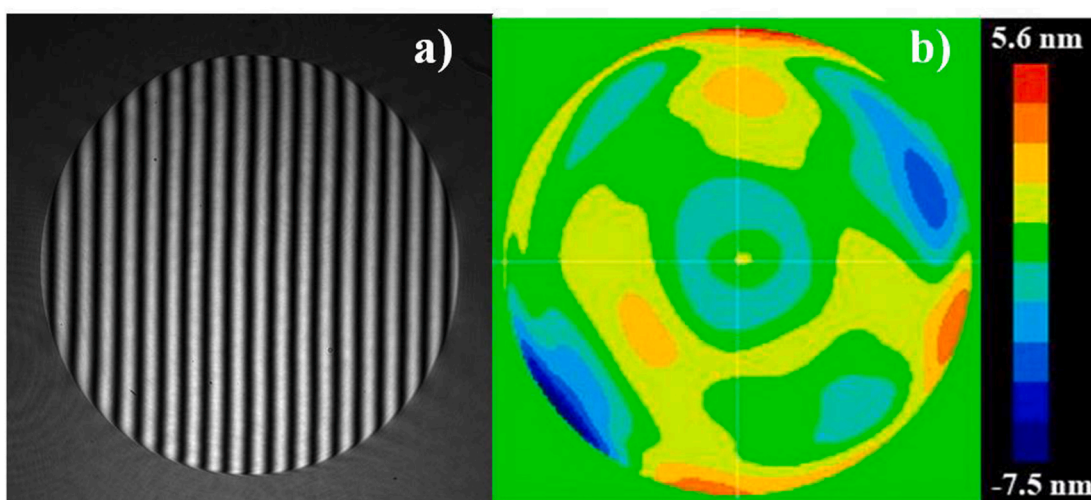
Fig. 11. Measured error map for the surface shape of the concave sphere of reference #2.

where $W_i(r)$ is the aberration from the i-*th* optical element. Thus, by minimising the functional in (6) at the expense of each element over several iterations, we can adjust the system with the required accuracy. The direct relationship between the Zernike polynomials and the main alignment errors is an additional advantage in this approach, and significantly simplifies the alignment procedure. For example, the co-efficients for the coma aberration not only represent the presence of shifts and skews in the optical elements relative to the optical axis, but also allow the directions of these shifts to be recognised. The spherical aberration represents errors in the placement of the optical elements along the optical axis. The displacement of one of the TSMOFs along the optical axis leads to the appearance of a defocusing aberration and astigmatism. It is therefore essential to minimise the corresponding co-efficients and then to monitor the overall aberration. Since mechanical adjustments mainly affect low-frequency aberrations, the amplitude mode of recording interferograms was used during tuning, as it was less sensitive to mechanical vibrations, matrix noise, and fluctuations in the light intensity.

4. Experimental results

After adjusting the recording part of the interferometer, the measurement accuracy of the interferometer was investigated using the working aperture specified for the Mitutoyo plano objective. The set of objectives was NA = 0.055, 0.14, and 0.28. The procedure consisted of measuring the aberration of the two TSMOFs, which were selected using

Table 1
Passport and measured values for the surface shapes of the references.

Parameter	Reference #1	Reference #2
Passport data		
NA	0.03	0.065
PV, nm	24.1	–
RMS, nm	4.4	–
Measured results		
PV, nm	22.9	13.1
RMS, nm	4.1	1.5

the method described in Section 3.1 for minimal aberration. The distance between the TSMOFs, the exit aperture of the objective, and the size of the sensitive area of the detector were 22 μm, 11 mm, and 6 × 6 mm², respectively. An example is presented in Fig. 9, which shows an interferogram and a map of the measured aberrations. The aberration parameters were an RMS value of 0.7 nm and a peak to valley (PV) deviation of 4.4 nm.

The dependence of the RMS wavefront aberration on the value of the numerical aperture is shown in red circles in Fig. 7. If we compare the aberration without the optical system, we can see that despite the fact that the interfering fronts pass through the system along close paths, a noticeable error is still introduced into the measurement results. This error must be taken into account during operation of the interferometer.

Figs. 10 and 11 show the results of our measurements of spherical
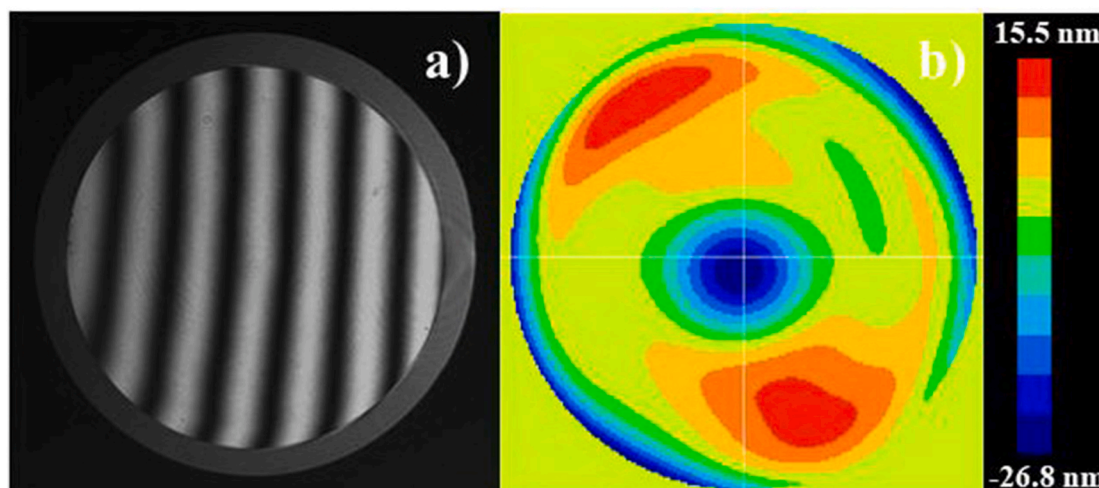
Fig. 12. Measured interferogram and aberration map for a five-element objective.

references provided by the two main suppliers on the world market. Reference #1 is also accompanied by a map of the surface error, as shown in Fig. 10(b). The available passport data for the references and the measurements are shown in Table 1. The following conclusions can be drawn from these. Firstly, a comparison can be made of the error maps for reference #1 in terms of the values measured in the current work and the data supplied by the manufacturer. We found that the results were comparable for both the shape measurements and the RMS and PV values. For reference #2, data from the supplier and an error map were not available, nevertheless, its high quality attracts the attention. The RMS aberration at 99% of the working aperture had a relatively low value of RMS = 1.52 nm or $\lambda/420$.

We note the simplicity of measurement of the lenses, using the interferometer coupled with a second coherent TSMOF (Fig. 3). Fig. 12 shows the interferogram and aberration map for a five-element projection lens with numerical aperture NA = 0.5, with aberration parameters PV = 42.3 nm and RMS = 8.2 nm. It can be seen that the main contributions are associated with spherical and coma aberrations. Since the lens was designed for the working wavelength of the interferometer, these errors may be due to inaccurate control over the distance between the elements and their centring while assembling the lens.

5. Discussion and conclusions

In this paper, we describe an interferometer based on a diffractive comparison wave, for which the overall dimensions, ease of maintenance and cost are comparable to those of conventional interferometers (for example the Fizeau type). This is achieved through the use of fibre-optic technologies and the integration of all elements into a single package. In contrast to traditional interferometers, our device reduces the need for calibrated reference surfaces due to the use of a spherical reference wave source based on a single-mode optical fibre with a sub-wavelength output aperture. This allows for a sub-nanometre level of measurement accuracy. The device offers the possibility of self-calibration based on the interference between the two sources of the reference spherical wave.

Another advantage of this interferometer is the elimination for the need for wavefront correctors while examining the lenses, projection lenses, Schwarzshild and Kirkpatrick-Baez optics, concave ellipsoids, and toroids. This is due to the presence of the second coherent source of the reference spherical wave, which can be placed at the focal point of the investigated object.

The numerical aperture of the interferometer can be increased by using a high-aperture objective with NA>0.28. This is mounted on a five-coordinate table for wavefront correctors, located at the output of

the interferometer. The lens is directly calibrated in the interferometer using a second source (Fig. 3).

The most important characteristic of any interferometer is the measurement accuracy. Numerous factors with a random nature (air flows, mechanical vibrations, instability of the radiation source, statistical fluctuations in the intensity of the registered light fluxes, etc.) may affect this accuracy. Random factors can reduce the contrast of the recorded interferograms and affect the reproducibility of measurements, and need to be recognised and either eliminated or minimised. The main sources of uncertainty in the measurement results of traditional interferometers are reference errors. Interferometers from the Zygo company, for example, provide a high relative level of measurement accuracy (measurement reproducibility) of up to $\lambda/10000$; However, the declared absolute measurement accuracy is at the level of $\lambda/20$–$\lambda/100$, and is determined by the reference used in the interferometer [2].

In addition to the errors introduced by the reference surface in traditional interferometers, the wavefront is transformed using additional optical elements into a converging or diverging spherical or flat front, which also introduces an uncontrollable error in the measurement results. In most cases, the user cannot double-check the declared characteristics of the interferometer, meaning that different interferometers often give different results, with an accuracy poorer than $\lambda/10$.

Our interferometer has a self-calibration function for the aberrations of the reference spherical wave and errors introduced by the recording part of the interferometer due to the possibility of carrying out an interference experiment with two TSMOFs (Fig. 8). From the results of this experiment, we can conclude that in the basic configuration, the measurement accuracy is around 0.7 nm for a numerical aperture NA = 0.28, and for smaller apertures, the accuracy is higher.

The measurement accuracy of the investigated object can be increased to sub-angstrom levels. This possibility of achieving this accuracy is associated with the joint processing of measurement results for different angles of rotation of the sample under study [13].

The interferometer described in this article, which has already been tested under industrial conditions to confirm the basic physical principles of operation, therefore represents a new type of instrument with a number of functions and capabilities that traditional commercial devices do not have, even in comparison with the PDI described in Ref. [10].

Declaration of competing interest

The authors declare that they have no known competing financial interests or personal relationships that could have appeared to influence the work reported in this paper.

Acknowledgments

References

[1] Malacara D, editor. Optical shop testing. second ed. New York: John Wiley&Sons, Inc.; 1992, ISBN 0-471-52232-5.

[2] https://www.zygo.com/products/metrology-systems/laser-interferometers/ver ifier.

[3] Williamson DM. In: Zernike F, Attwood DT, editors. The elusive diffraction limit, OSA proceedings on extreme ultraviolet lithography, vol. 23; 1995. p. 68–76. 1995.

[4] Linnik VP. Simple interferometer for the investigation of optical systems. Bull Acad Sci USSR 1933;1:208–10.

[5] Sommargren GE. Diffraction methods raise interferometer accuracy. Laser Focus World 1996;8:61–71.

[6] Medecki H, Tejnil E, Goldberg KA, Bokor J. Phase-shifting point diffraction interferometer. Opt Lett 1996;21(19):1526–8. https://doi.org/10.1364/OL.21.001526.

[7] Naulleau PP, Goldberg KA, Lee SH, Chang C, Attwood D, Bokor J. Extreme-ultraviolet phase-shifting point-diffraction interferometer: a wave-front metrology tool with subangstrom reference-wave accuracy. Appl Opt 1999;38(35):7252–63. https://doi.org/10.1364/AO.38.007252.

[8] Otaki K, Ota K, Nishiyama I, Yamamoto T, Fukuda Y, Okazaki S. Development of the point diffraction interferometer for extreme ultraviolet lithography: design, fabrication, and evaluation. J. Vac. Sci. Technol B 2002;20(6):2449–58. https://doi.org/10.1116/1.1526605.

[9] Nikolay B, Voznesensky, Kyeong Hee Lee, Vladimir K, Kirillovsky. Principle of highest-precision optical parts estimation on the basis of a point-diffraction interferometer. Proc. SPIE 5252, Optical Fabrication, Testing, and Metrology 2004. https://doi.org/10.1117/12.512231. 26 February.

[10] Difrotec D7 interferometer. http://media.voog.com/0000/0037/7881/files/Difro tec_Brochure_Product%26Services_medQ.pdf.

[11] Chkhalo NI, Klimov A Yu, Rogov VV, Salashchenko NN, Toropov MN. A source of a reference spherical wave based on a single mode optical fiber with a narrowed exit aperture. Rev Sci Instrum 2008;79:033107. https://doi.org/10.1063/1.2900561.

[12] Wang D, Chen X, Xu Y, Wang F, Kong M, Zhao J, Zhang B. High-NA fiber point-diffraction interferometer for three-dimensional coordinate measurement. Opt Express 2014;22(21):25550–9. https://doi.org/10.1364/OE.22.025550.

[13] Chkhalo NI, Malyshev IV, Pestov AE, Polkovnikov VN, Salashchenko NN, Toropov MN, Soloviev AA. Problems in the application of null lens for precise measurements of aspheric mirrors. Appl Opt 2016;55(3):619–25. https://doi.org/10.1364/AO.55.000619.

[14] Svechnikov MV, Chkhalo NI, Toropov MN, Salashchenko NN, Zorina MV. Application of point diffraction interferometry for middle spatial frequency roughness detection. Opt Lett 2015;40(2):159–62. https://doi.org/10.1364/OL.40.000159.

[15] Rhee H-G, Kim S-W. Absolute distance measurement by two-point-diffraction interferometry. Appl Opt 2002;41(28):5921–8. https://doi.org/10.1364/AO.41.005921.

[16] Wang D, Xu Y, Liang R, Kong M, Zhao J, Zhang B, Li W. High-precision method for submicron-aperture fiber point-diffraction wavefront measurement. Opt Express 2016;24(7):7079–90. https://doi.org/10.1364/OE.24.007079.

[17] Dryakhlushin VF, Klimov A Yu, Rogov VV, Gusev SA. Scanning near-field optical microscope probe. Devices and Technique of Experiment 1998;2:138–9 [In Russian)].

[18] Chkhalo NI, Malyshev IV, Pestov AE, Polkovnikov VN, Salashchenko NN, Toropov MN. Diffraction limited X-ray optics: technology, metrology, applications. Phys Usp 2020;63(1):67–82. https://doi.org/10.3367/UFNe.2019.05.038601.

[19] Dai G-M. Zernike aberration coefficients transformed to and from Fourier series coefficients for wavefront representation. Opt Lett 2006;31(4):501–3. https://doi.org/10.1364/OL.31.000501.